Measurement of the transverse momentum dependence of the elliptic flow of charged particles in lead-lead collisions at $\sqrt{s_{NN}} = 2.76$ TeV

Pouria Jaberi

Supervisor: Peter Christiansen

LUND
UNIVERSITY

Particle Physics Division
Department of Physics
Lund University
Januari, 2013

Contents

Chapter 1

1 Introduction

Particle physics is a basic field of science that can answer to some questions referred to as "What is matter made of?" , "What are the smallest building blocks in the universe?", and so on. At subatomic level matter is made of remarkable tiny "chunks" with a large space of vacuum between them. In the field of particle physics, the standard model is the famous theory that explains the elementary particles and their interactions. In this chapter I will summarize the main points of this theory relevant for my project.

1.1 The Standard Model (SM)

The SM divides particles into three groups: quarks, leptons and gauge bosons. The two first groups are fermions (matter particles) and the third group is bosons which describes the forces of nature. The four forces of nature are: the electromagnetic force, the weak force, the strong force and the gravitational force. Except for the gravitational force, which is the weakest, all other forces have been studied in microscopic experiments. Quantum Cromodynamics (QCD) describes the strong interaction. The electromagnetic interaction and the weak interaction can be described by the Glashow-Weinberg-Salam electroweak theory. General relativity describes the gravitational interaction but there is no quantum field theory for gravity yet. In the following we only mention the three forces described by the SM.

The six quarks in the SM are up, down, charm, strange, top and bottom. The six leptons are electron, electron neutrino, muon, muon neutrino, tau, tau neutrino. The quarks and leptons can be divided into three generations with different masses but otherwise similar characteristic such as spin, color, handedness, etc. The quarks are affected by all three forces but the leptons interact with just electroweak interaction.

The forces in the SM are explained by the exchange of virtual gauge bosons between the fermions. The massless photon is responsible for the electromagnetic interaction. The W^+, W^- and Z bosons are responsible for weak interaction and massless gluons are responsible for strong interaction. Figure 1.1 summarizes Standard Model particles in a table. All of the particles also have anti-particles. The anti-particles of fermions have the same characteristic as their particles but the opposite charge. The photon, gluon and Z have no distinguishable anti-particle. The W^+ has the anti-particle W^-.

1.2 Quantum Chromodynamics

Quantum Chromodynamics (QCD) is the SM theory for the strong force which explains the strong interaction between quarks as mediated by gluons. QCD is a quantum field theory of a non-abelian gauge theory where gluon bosons are exchanged between quark color fields. In the real world, quarks are confined by the gluon fields and there exist no free quarks. In the electromagnetic interaction the charge can be positive or negative. For the color charge of quarks, the charges can be red (r), green (g) and blue (b) and for antiquarks, the charges can

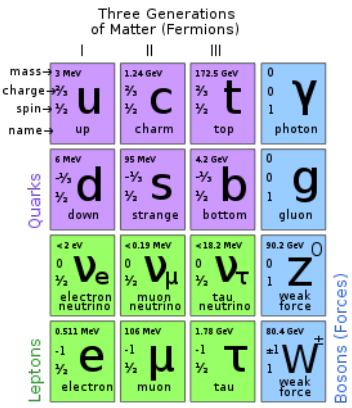

Figure 1.1: The Standard Model particles. The three first columns are the three generation of particles. The fourth column shows the gauge bosons [17].

be anti-red ($\bar{r}$), anti-green ($\bar{g}$) and anti-blue ($\bar{b}$). Quarks can combine together to form hadrons. Hadrons can consist of three quarks that is called a baryon or consist of two quarks (one quark and one anti-quark) that is called a meson.

The strong interaction has two different properties from other forces: confinement and asymptotic freedom.

1.Confinement: Where gravity and electroweak interaction become weaker when the distance is increased, the strong interaction becomes stronger. Figure 1.2 shows the quark-quark potential. The strong force potential increases with the distance between the two quarks. Thus if two quarks come far from each other, the force between them increases like if a rubber band would connect them. So it takes a high energy to separate two quarks and it is not possible to have free quarks.

2.Asymptotic freedom: At very short distances (large energy transfers), the strong force acts weakly, so that quarks and gluons inside a hadron appears to be free. This happens in high energy collisions. Asymptotic freedom was formulated by Frank Wilczek, David Gross, and David Politzer who won the nobel prize in 2004.

1.3 Quark-Gluon Plasma

In 1974 at a workshop in Bear Mountain, New York, T.D.Lee proposed that at high energy densities, it is possible to have a new state of matter where the quarks are deconfined. The Quark-Gluon Plasma (QGP) is a very dense state of matter where quarks and gluons are deconfined. Today quarks are bound together by gluons, but 1 μs after the big bang the universe was in the phase of QGP with a high temperature and high density. Figure 1.3 shows a schematic view of the evolution of the universe from the big bang until now.

To study this phase of asymptotic freedom theorists uses Latice QCD (lQCD). Latice QCD is a tool to solve the non-perturbative theory of Quantum Chromodynamics numerically. These simulations predict that the temperature of the phase transition is 170 GeV or an energy density of 1 GeV/fm^3. A schematic view of the QCD phase diagram is shown in figure 1.4. This shows the cooling trajectory of the universe and how we hope to recreate this new phase of matter by colliding nuclei.

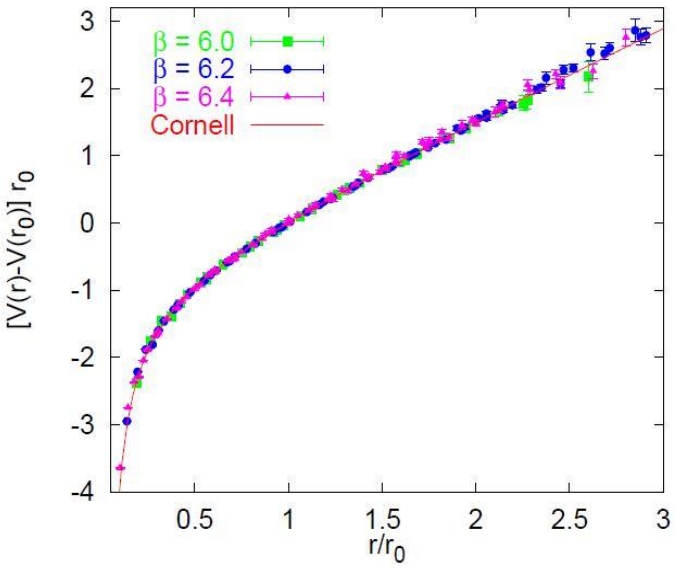

Figure 1.2: The quark-quark potential extracted from lattice QCD [18].

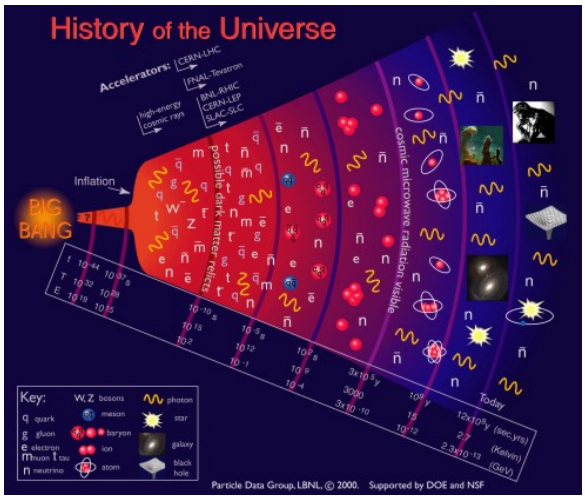

Figure 1.3: The evolution of matter in the universe from the Big Bang [19].

1.4 Heavy Ion Collision

In order to study the Quark-Gluon plasma, we need to be able to create it in the laboratory. Particle accelerators usually use electron or proton collisions to study the new particles, but to create a "microscopic" QGP, heavy ion collisions are needed. The nuclei used in heavy ion collisions is gold (Au) or lead (Pb). This is done near New York at the Brookhaven National Laboratory (BNL) at the Relativistic Heavy Ion Collider (RHIC) and in CERN at the LHC (Large Hadron Collider).

Unfortunately, it is not possible to observe the medium directly in the collision, as in each event, it exists for a very short time ($10^{-23}s$) before it hadronises to normal hadronic matter. Therefore, the only way that can be used to study this phase is to measure the outgoing particles. The kinematic properties of the outgoing particles can give us the information about the medium. In order to understand characteristic of the medium, it is not enough to consider a single occurrence of a very short lived QGP. In addition, the quantum theory in this scale is statistical in nature, therefore, to get better results many heavy ion collisions are needed.

To describe the phase of QGP we first need to define some references. A good start is

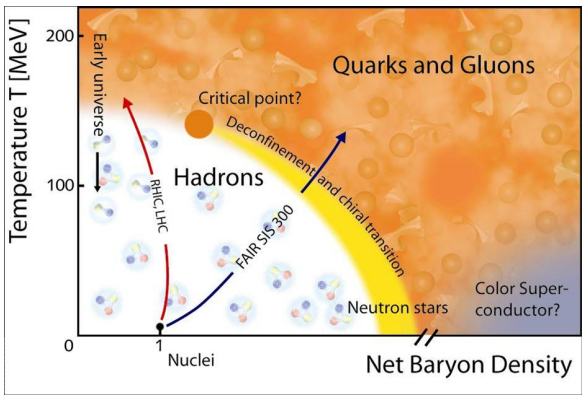

Figure 1.4: Schematic of the QCD phase. It shows the evolution of baryonic state vs. temperature [20].

a reaction plane xz, as shown in figure 1.5. In a simple picture, the two nuclei are spherical and the reaction plane is along the beam axis. The region of interaction of the two nuclei has roughly an almond shape perpendicular to the reaction plane.

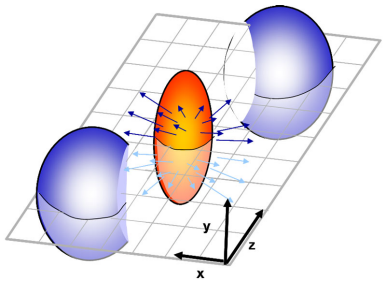

Figure 1.5: Colliding two heavy ions can create an ellipsoidal spectator fireball and two remnants with spectator [21].

An important factor, the centrality, defines how much the collision is central in percentage. In other words, it indicates the amount of nucleons participating in collision. If the centrality is low, it is called a central collision, which means that most of the nucleons are participating in the collision. If the centrality is high, it is called a peripheral collision with a few nucleons interacting on the edges of nuclei only. These values are evaluated from the number of charged particles which are produced from collision using the Glauber model (Figure 1.6).

1.5 Transverse Momentum

One of the important kinematics factors in particle physics is the transverse momentum of particles. The momentum of outgoing particle has two parts: a transverse momentum (p_t) and a parallel momentum (p_z). The transverse momentum is invariant under a lorentz boost along the beam axis transformation and can be defined as:

$$p_t = \sqrt{p_x^2 + p_y^2} \tag{1.1}$$

It is particularly interesting as the p_t of the two nuclei is 0, so that the p_t of detected particles is generated in the collision.

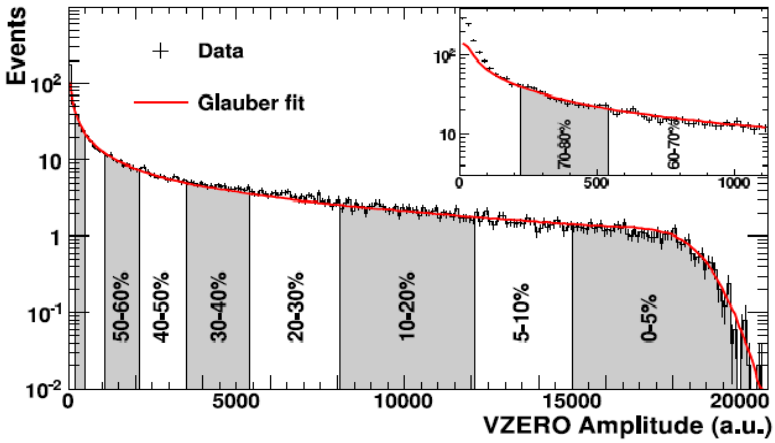

Figure 1.6: Glauber fit to the charged particle distribution showing the different centrality classes [14].

Chapter 2

2 Experiment

In this chapter experimental facilities used in this thesis are described. First the LHC at CERN is explained. Then the ALICE detector which is used for the study of heavy ion collisions is described.

2.1 The Large Hadron Collider

The LHC is located at the European Organization for Nuclear Research (French: Organization européenne pour la recherche nucléaire), famous as CERN. It is near Geneva, on the border between France and Switzerland and it is the most important and the biggest particle physics accelerator in the world. The circumference is 27 km and it is built 100 meter under ground. The accelerator is built for colliding proton-proton and heavy ions. The energy in the center of mass for pp collision is up to 7 TeV and for heavy ion collision is 2.76 TeV per nucleon pair.

There are several unanswered principle questions that the LHC has been built to find an answer to. These are some of the questions:

- The test of Higgs mechanism according to electroweak symmetry breaking and the existence of Higgs particle.
- What is the nature of dark matter and dark energy? We only can observe that 4% of the universe is SM matter but what does the other part of the universe consist of?
- Why is matter dominant over antimatter in the universe?
- What is the nature of the Quark-Gluon plasma?
- Are there extra dimensions in the universe? This can be a test of string theory.
- The electroweak force is the combination of electromagnetism and weak interaction. Can the strong force be combined with this force? Are the Grand Unification Theories correct?
- What is the origin of gravity? and why is it the weakest force among the four fundamental forces?
- Does the particles of the Standard Model have other partners? In the supersymmetry theory (an extension of Standard Model) is the prediction of supersymmetric partners.
- Are there more generations in the Standard Model?

To investigate these issues four detectors have been built at four different locations in the LHC ring. ATLAS (A Toroidal Lhc ApparatuS) and CMS (Compact Muon Solenoid) are the two detectors which are the largest among the four. The purpose of these detectors is to find new particles, to test the predictions of supersymmetry and to discover of new physics beyond

the standard model. The main focus of these experiments is proton-proton collisions. The LHCb is designed to study CP violation in bottom quark physics to investigate the assymetry between the matter and antimatter. Finally, ALICE (A Large Ion Collider Experiment) is designed to study the QGP in heavy ion physics: Pb-Pb collisions. Figure 2.1 shows the LHC ring with the four detectors located.

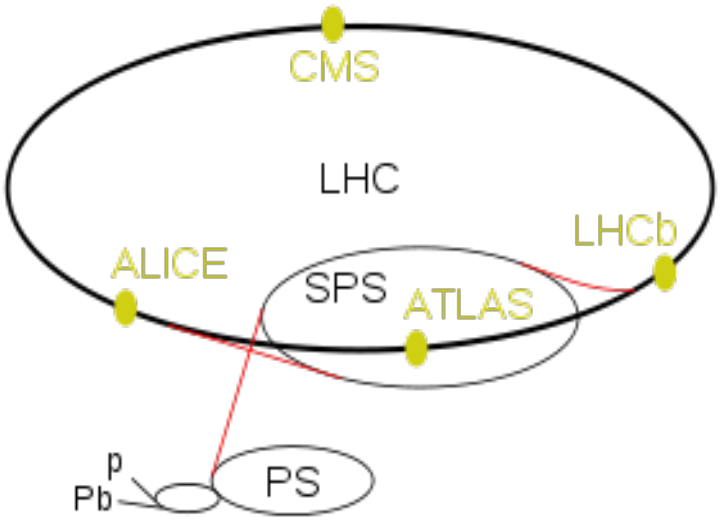

Figure 2.1: A schematic diagram of the LHC accelerator with the four main detectors [22].

2.2 ALICE

ALICE (A Large Ion Collider Experiment) is the main detector at LHC for the study of heavy ion physics. It has been designed to investigate the strong force and the quark-gluon plasma. The dimensions of this detector is $16 \times 16 \times 26$ m^3 and the weight is approximately 10000 tons. In heavy ion collision more particles can be produced than in pp collision but the interaction rate is smaller than for proton collisions. The design interaction rate in Pb-Pb collision is 1 kHz but in proton-proton collision it is 40 MHz. The lower rate requirements has influenced the ALICE detector technologies and has allowed the use of a "slow" Time Projection Chamber as the main tracking device, see below. ALICE is able to measure and identify with good performance low transverse momentum particles. Figure 2.2 shows the ALICE detector.

The ALICE detector has two main parts. The first part is the L3 magnet and the detectors inside it (left part of figure 2.2). This part is called the central barrel and is the part used in this thesis. The other part is the muon spectrometer which consists of an absorber, a tracker and a trigger.

The different detectors are designed for different purposes. The ITS (Inner Tracking System) is the closest detector to the interaction point, and provides information on tracking and identification of low p_t particles. ITS has three different parts. SPD (Silicon Pixel Detector), SDD (Silicon Drift Detector) and SSD (Silicon Strip Detector). Outside of the ITS is the TPC (Time Projection Chamber). It consist of a gas chamber with a volume of approximately 90 m^3. The TPC is followed by three particle identification detectors: TRD (Transition Radiation Detector), TOF (Time Of Flight) detector and HMPID (High-Momentum Particle Identification Detector). TRD discriminates electrons from pions with a high efficiency. TOF allows to identify pions, kaons and protons at low and intermediate p_t. The HMPID is a ring imaging Cherenkov radiation detector.

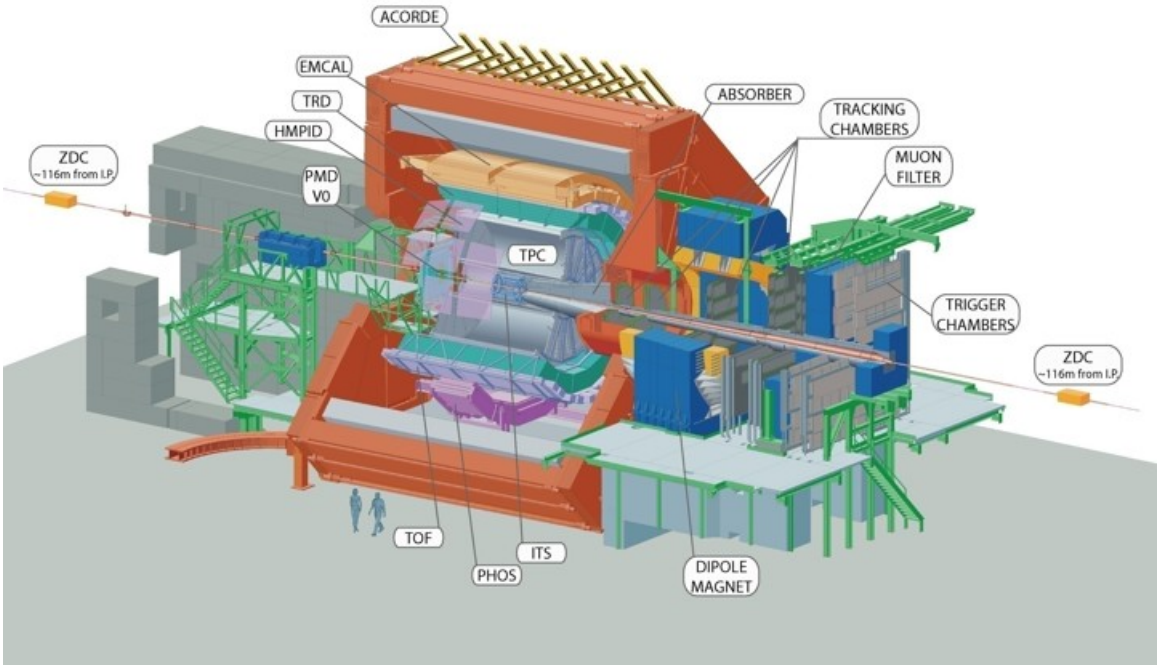

Figure 2.2: The ALICE experiment [23]

2.3 The Time Projection Chamber(TPC)

The Time Projection Chamber (TPC) is a detector which was invented in the 1970s for tracking the charged particles in three dimensions. It provides in addition to tracking a measurement of the energy loss, dE/dx, of the particles. The detector is shaped as a hollow cylinder filled with gas and a uniform electric field that is created from the two end plates to the central cathode. The magnetic field of the L3 magnet is parallel to the electric field (and the beam lines). The end caps of the cylinder are instrumented with sensitive anode wire chambers covered by cathode pads. The ALICE TPC is the largest in the world.

The principle of the TPC is based on that the charged particles passing through the gas-filled cylinder ionize the gas atoms and the freed electrons drift towards the anode because of the electric field. When detecting the electrons, the particle's trajectory can be reconstructed: arrival measuring the projection of the track on the end plate, the time of flight of the electrons. Knowing the drift velocity of the electron, the 3-dimensional trajectory of the particle can be determined. Besides, we can measure the momentum of the particle from the curvature of the track in the magnetic field. The mass of the particle can also be measured with some precision knowing the energy loss. Figure 2.3 shows the schematic of the TPC and figure 2.4 shows tracks from a single event in the TPC in a lead-lead collision. In this thesis we used the data of the TPC of the ALICE experiment.

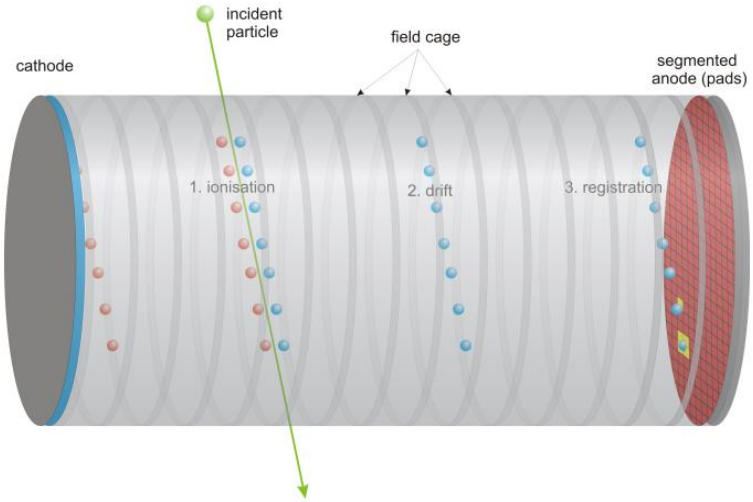

Figure 2.3: Illustration of TPC working principle. The charged particles pass the cylinder and free electrons drift to the anode pads. Note that this is not the ALICE TPC [15].

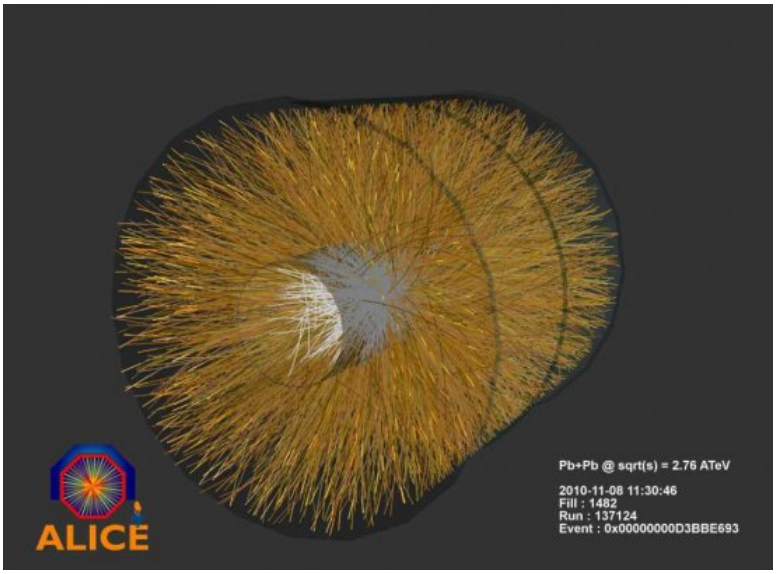

Figure 2.4: Event display for a central Pb-Pb collision. Tracks from charged particles as reconstructed in the ALICE TPC [24].

Chapter 3

3 Flow

An important subject in heavy ion research is flow. Figure 3.1 shows a non-central collision of two nuclei in the transverse plane. The participants of the collision are distributed in an almond shape region at an angle with respect to the horizontal plane called the reaction plane angle, Ψ_R. Due to pressure gradients, the pressure along the minor axis is larger than the pressure along the major axis. If hydrodynamics can be used to describe the system, this pressure difference will convert a spatial anisotropy into a momentum anisotropy: elliptic flow. This azimuthal anisotropy is the result of hydrodynamical behavior in the quark-gluon plasma.

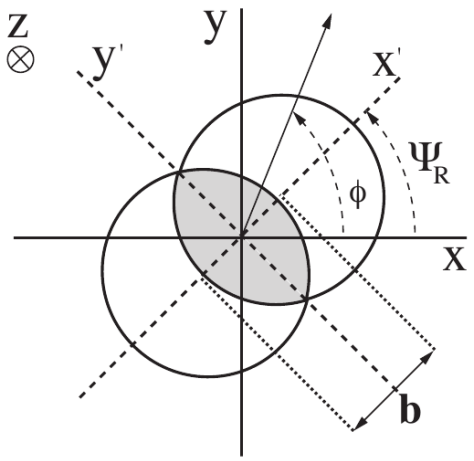

Figure 3.1: Schematic view of a non-central nucleus-nucleus collision. The shadowed region is the active participant part of the collision which in this figure is almond shape and gives rise to the elliptic flow [25].

3.1 Fourier Expansion of Azimuthal Distribution

In 1994 Voloshin and Zhang suggested using Fourier series expansion for azimuthal anisotropy analysis. This method has some advantages. It has sine and cosine terms and is described by a periodic function. Voloshin and Zhang denoted the azimuthal distribution function, r(ϕ), where ϕ is the azimuthal angle of particles emitted after collision. The r(ϕ) can be constructed event by event in the form of a Fourier expansion:

$$r(\phi) = \frac{1}{2\pi} + \frac{1}{2\pi}\sum_{n=1}^{\infty}[x_n \cos(n\phi) + y_n \sin(n\phi)] \tag{3.1}$$

The coefficients x_n and y_n are in the integral form of Fourier expansion. For a finite number of particles, the integral runs over all particles, so coefficients become:

$$x_n = \int_0^{2\pi} r(\phi)\cos(n\phi)d\phi = \sum_\nu r_\nu \cos(n\phi_\nu) \tag{3.2}$$

$$y_n = \int_0^{2\pi} r(\phi)\sin(n\phi)d\phi = \sum_\nu r_\nu \sin(n\phi_\nu) \tag{3.3}$$

where ν runs over all particles and ϕ_ν is the azimuthal angle of the particle. Each of the non-zero pair of Fourier coefficient can be defined as:

$$x_n = v_n \cos(n\Psi_n) \tag{3.4}$$

$$y_n = v_n \sin(n\Psi_n) \tag{3.5}$$

where Ψ_n is the reaction plane angle of n-th particle. The n-th order flow coefficient is then expressed as:

$$v_n = \sqrt{x_n^2 + y_n^2} \tag{3.6}$$

3.2 Anisotropic Azimuthal Flow

Using the Fourier expansion relative to the reaction plane angle gives us different orders of anisotropic flow:

$$\begin{aligned} E\frac{d^3N}{dp^3} &= \frac{1}{2\pi}\frac{d^2N}{p_t dp_t dy}\left(1 + \sum_{n=1}^{\infty} 2v_n \cos[n(\phi - \Psi_R)]\right) \\ &= \frac{1}{2\pi}\frac{d^2N}{p_t dp_t dy}(1 + 2v_1\cos(\phi - \Psi_R) + 2v_2\cos(\phi - \Psi_R) + ...) \end{aligned} \tag{3.7}$$

where ϕ is the azimuthal angle, v_n is flow (v_1 is directed flow, v_2 is elliptic flow, v_3 is triangular flow and so on), p_t is transverse momentum, y is the rapidity and Ψ_R is the reaction plane angle. For many years it was argued that at midrapidity, $\eta = 0$, all uneven v_n were 0 due to symmetry. This is true for Ψ_R. However in 2010 Alver and Roland showed that there exists Ψ_3 generated by fluctuations in the initial state that can give large v_3 [12].

Figure 3.2 shows the v_2 moment or elliptic flow but in reality it is not as simple as this figure.

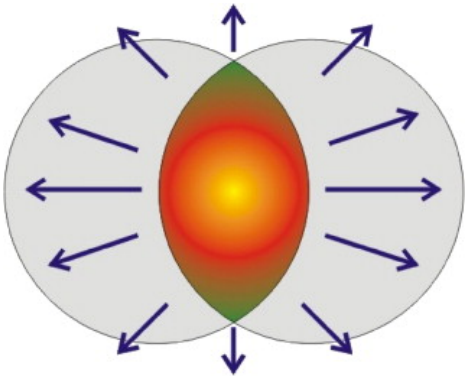

Figure 3.2: A simple schematic view of how elliptic flow is generated in a non-central collision of two nuclei [26].

Figure 3.3 shows a simulation of a Pb-Pb collision at $\sqrt{s_{NN}} = 2.76$ TeV with the PHOBOS Glauber Monte Carlo. In the left panel full circles show participating nucleons and dotted circles show the spectators. The right panel is the same simulation with showing the orders of higher eccentricities, ε_1, ε_2, ε_3, ε_4,..., that are responsible for generating the flow gradients.

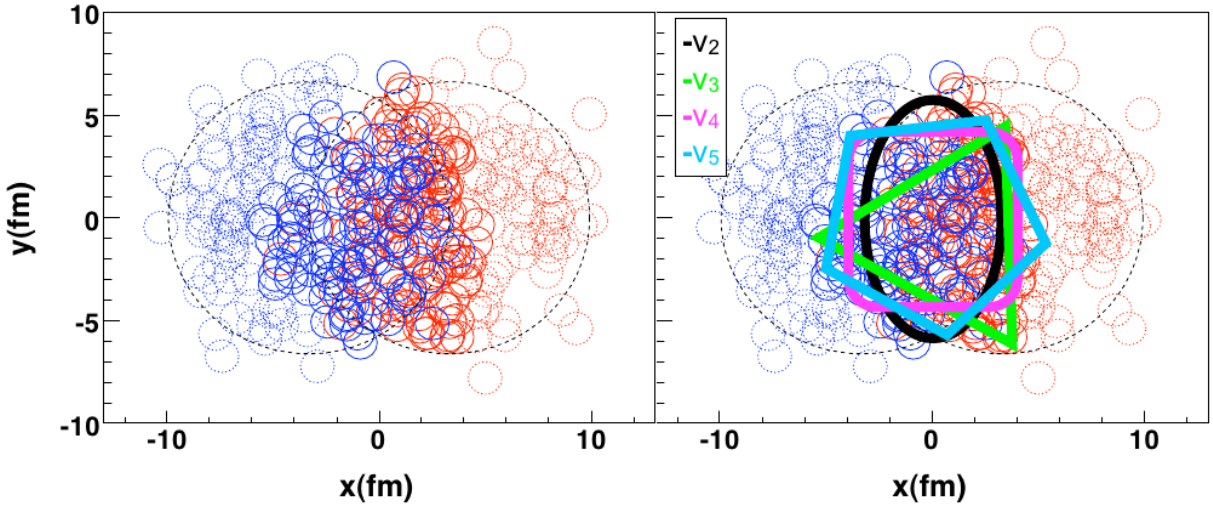

Figure 3.3: Simulation of Pb-Pb collision at $\sqrt{s_{NN}} = 2.76$ TeV with the PHOBOS Glauber Monte Carlo. The right panel shows the shaping of n-th moment of flow [16].

3.3 Elliptic flow

The aim of this thesis is to measure elliptic flow, v_2, as a function of transverse momentum. Figure 3.4 shows official results for elliptic flow at different centralities measured with the ALICE data. The v_2 is integrated over 0.2 GeV/c $< p_t <$ 5 GeV/c. For most central collision the elliptic flow is small. The maximum value of v_2 is at the medium centrality (about 40%-60%).

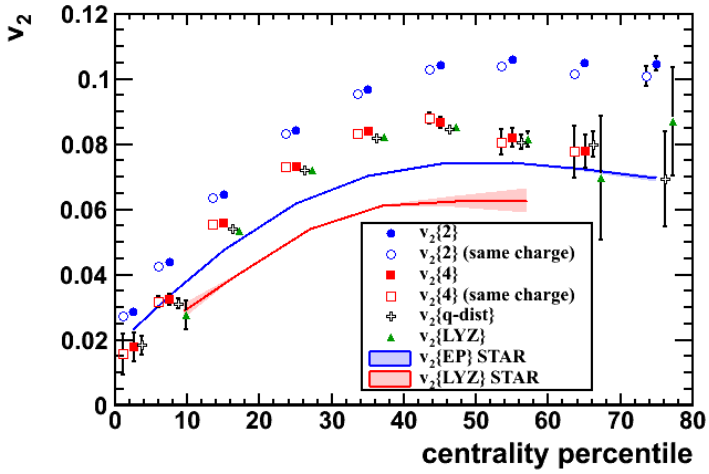

Figure 3.4: v_2 for 0.2 GeV/c $< p_t <$ 5 GeV/c for different centrality bins [2].

Figure 3.5 shows the elliptic flow as a function of transverse momentum measured at the LHC and at RHIC. In the upper panel two different methods are used to measure elliptic flow at the different centrality 40%-50%. Blue stars show v_2 obtained using the 2-particle cumulant method and red triangles using the 4-particle cumulant method. The lower figure shows $v_2(p_t)$ 4-particle cumulant for several centrality bins. The maximum value of v_2 is at around 3-4 GeV.

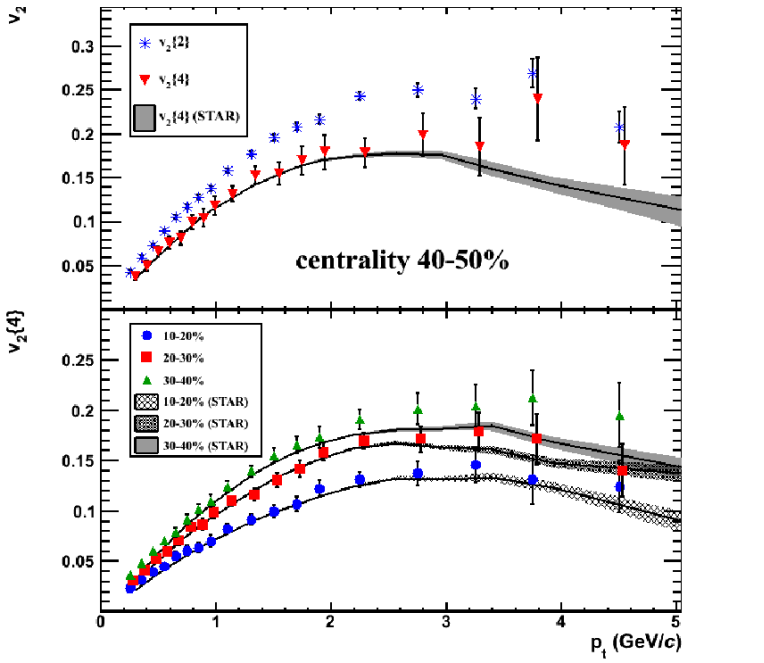

Figure 3.5: Elliptic flow as a function of transverse momentum(p_t) measured at LHC and at RHIC. Note that different methods were used to measure v_2 at LHC and RHIC [2].

Chapter 4

4 Method

As mentioned in the previous chapter, in heavy ion research different orders of flow can be measured. The first order is called directed flow, the second order is elliptic flow, the third order is triangular flow and so on. The main purpose of this thesis is to measure elliptic flow coefficient, v_2. There are different methods to measure the elliptic flow. First I explain the event plane method and then the Q-cumulant method.
We will begin by writing differential particle yield in Fourier expansion:

$$\frac{d^3N}{dp_t^2 d\phi dy} = \frac{1}{2\pi}\frac{d^2N}{p_t dp_t dy}[1 + 2v_2\cos(\phi - \Psi_R)] \tag{4.1}$$

where ϕ is azimuthal angle, v_2 is elliptic flow, p_t is transverse momentum, y is rapidity and Ψ_R is the reaction plane angle. The elliptic flow coefficient, v_2, can be expressed as:

$$v_2 = \langle\cos[2(\phi - \Psi_r)]\rangle \tag{4.2}$$

where Ψ_r is the reaction plane angle and the average is over all of the particles in all the events. The problem of determining elliptic flow this way is that the reaction plane angle cannot be well determined experimentally. However, different methods are suggested to solve this problem. The two main methods are the event plane method and Q-cumulant.

4.1 The Event Plane Method

The reaction plane angle cannot be calculated experimentally. Voloshin and Zhang suggested a method to measure the event plane instead of measuring the reaction plane. The observed event plane, Ψ^{obs} or Ψ_2 can be substituted by reaction plane angle. To determine the Ψ^{obs}, the elliptic flow vector, $\overrightarrow{Q_2}$, is constructed.

$$Q_2^x + iQ_2^y = \sum_{i=1}^{M} e^{2i\phi_i} \tag{4.3}$$

where i runs over all particles in all events and Q-value is calculated with a loop of all the particles. Q-value has two components with respect to the azimuthal angle. The event plane angle of 2nd harmonic can be determined by:

$$\Psi_2 = \frac{1}{2}\tan^{-1}\left(\frac{Q_2^y}{Q_2^x}\right) = \frac{1}{2}\tan^{-1}\left(\frac{\sum_i \sin(2\phi_i)}{\sum_i \cos(2\phi_i)}\right) \tag{4.4}$$

where $\Psi_2 \in [\frac{-\pi}{2}, \frac{\pi}{2})$
The observed elliptic flow has a lower magnitude than the "actual" elliptic flow because of the

event plane angle smearing and with respect to reaction plane has different value. The 2nd harmonic of observed flow is:

$$v_2^{obs} = \langle \cos[2(\phi - \Psi_2)] \rangle \tag{4.5}$$

Figure 4.1 shows the v_2 from the event plane method obtained in this analysis with comparison to ATLAS data in the centrality bin 30%-40%.

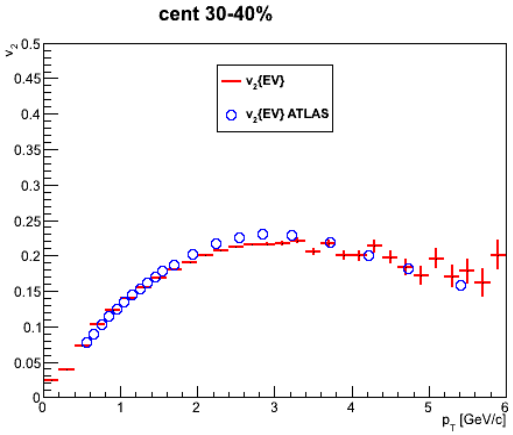

Figure 4.1: Elliptic flow (event plane method) as a function of transverse momentum (p_T) in the centrality 30%-40%.

4.2 Particle Cumulant

The cumulant method has two advantages over the event plane method. Reaction (event) planes need not to be known and the method can be expanded to multi-particle correlations. Multi-particle correlations are less affected by non-flow effects, which are caused by particle correlations that are not directly related to the reaction plane, such as jet-correlation and resonance decays [9]. In general, non-flow is a few-body correlation while flow is a many-body correlation (via the reaction plane). It was suggested that non-flow effects are largely canceled in a particular combination of two- and four-particle correlations [10,11]. In multi-particle correlations, the extracted elliptic flow behaves differently under fluctuations. In the cumulant method, event plane is not used, but another reference is needed for integrated flow (reference flow). In this thesis, the goal is to measure integrated v_2 over a large part of phase space and differential flow, $v_2(p_T)$, for a particle of interest, as a function of transverse momentum using both 2-particle and 4-particle cumulants.

In this method we don't use the event plane angle, but rather the flow is measured by azimuthal correlations of observed particles. The elliptic flow of two particle azimuthal correlation can be justified by:

$$\begin{aligned}
\langle \cos[2(\phi_1 - \phi_2)] \rangle = \langle e^{2i(\phi_1 - \phi_2)} \rangle &= \langle e^{2i(\phi_1 - \phi_2 + \psi_{RP} - \psi_{RP})} \rangle \\
&\simeq \langle e^{2i(\phi_1 - \psi_{RP})} \rangle \langle e^{2i(\phi_2 - \psi_{RP})} \rangle \\
&\simeq \langle \cos[2(\phi_1 - \psi_{RP})] \rangle \langle \cos[2(\phi_1 - \psi_{RP})] \rangle \\
&= v_2 v_2 \\
&= v_2^2
\end{aligned} \tag{4.6}$$

In general, the non-flow effects are not negligible. However, when using the multi-particle correlations, the non-flow contribution is negligible. The problem of using multi-particle correlations is to loop over all the possible particle multiplets. To solve this problem, the elliptic flow vector is defined using the same equation in 4.3. With the introducing of the Q-vector, the elliptic flow coefficient can be measured. First, the 2-particle and 4-particle reference elliptic flow measuring the integrated flow is defined, then the differential elliptic flow is explained using particles of interest.

4.2.1 Two Particle Elliptic Flow

The definition of the two particle azimuthal correlation is:

$$\langle 2 \rangle \equiv \langle e^{2i(\phi_1 - \phi_2)} \rangle \equiv \frac{1}{P_{M,2}} \sum_{i=1}^{M} \sum_{j=1(j \neq i)}^{M} e^{2i(\phi_i - \phi_j)} \tag{4.7}$$

where $P_{n,m} = n!/(n-m)!$ and the sum is over different taken values. To obtain the second order cumulant, we start by constructing $\mid Q_2 \mid^2$:

$$\mid Q_2 \mid^2 = Q_2 Q_2^* = \sum_{i,j=1}^{M} e^{2i(\phi_i - \phi_j)} = M + \sum_{i=1}^{M} \sum_{j=1(j \neq i)}^{M} e^{2i(\phi_i - \phi_j)} \tag{4.8}$$

The two particle azimuthal correlation can then be calculated:

$$\langle 2 \rangle = \frac{\mid Q_2 \mid^2 - M}{M(M-1)} \tag{4.9}$$

and it should be averaged over all events:

$$\langle\langle 2 \rangle\rangle = \langle\langle e^{2i(\phi_1 - \phi_2)} \rangle\rangle = \frac{\sum_{i=1}^{N} (W_{\langle 2 \rangle})_i \langle 2 \rangle_i}{\sum_{i=1}^{N} (W_{\langle 2 \rangle})_i} \tag{4.10}$$

where $W_{\langle 2 \rangle}$ is an event weight defined as:

$$W_{\langle 2 \rangle} = M(M-1) \tag{4.11}$$

The second order cumulant is:

$$c_2\{2\} = \langle\langle 2 \rangle\rangle \tag{4.12}$$

The elliptic flow obtained from 2-particle correlations can then be derived as:

$$v_2\{2\} = \sqrt{c_2\{2\}} \tag{4.13}$$

4.2.2 Four Particle Elliptic Flow

The elliptic flow moment of 4-particle cumulant is more complicated than for 2-particle cumulant. The starting point is to define the four particle azimuthal correlation:

$$\langle 4 \rangle \equiv \langle e^{2i(\phi_1 + \phi_2 - \phi_3 - \phi_4)} \rangle \equiv \frac{1}{P_{M,4}} \sum_{i,j,k,l=1}^{M} e^{2i(\phi_1 + \phi_2 - \phi_3 - \phi_4)} \tag{4.14}$$

The sum is over different taken value. Then, to derive the 4-particle elliptic flow, the $\mid Q_2 \mid^2$ is constructed:

$$\mid Q_2 \mid^4 = Q_2 Q_2 Q_2^* Q_2^* = \sum_{i,j,k,l=1}^{M} e^{2i(\phi_i + \phi_j - \phi_k - \phi_l)} \tag{4.15}$$

The calculation of sum is complicated here because of 4 indices if they are equivalent or not. The four particle correlation is found to be:

$$\langle 4 \rangle = \frac{\mid Q_2 \mid^4 + \mid Q_4 \mid^2 - 2.Re[Q_4 Q_2^* Q_2^*]}{M(M-1)(M-2)(M-3)} - 2\frac{2(M-2).\mid Q_2 \mid^2 - M(M-3)}{M(M-1)(M-2)(M-3)} \tag{4.16}$$

Averaging over N events yield:

$$\langle\langle 4 \rangle\rangle = \langle\langle e^{2i(\phi_1 + \phi_2 - \phi_3 + \phi_4)} \rangle\rangle = \frac{\sum_{i=1}^{N} (W_{\langle 4 \rangle})_i \langle 4 \rangle_i}{\sum_{i=1}^{N} (W_{\langle 4 \rangle})_i} \tag{4.17}$$

where $W_{\langle 4 \rangle}$ is an event weight:

$$W_{\langle 4 \rangle} = M(M-1)(M-2)(M-3) \tag{4.18}$$

The forth order cumulant can be calculated:

$$c_2\{4\} = \langle\langle 4 \rangle\rangle - 2\langle\langle 2 \rangle\rangle^2 \tag{4.19}$$

Finally the elliptic flow obtained from four particle correlations can be derived as:

$$v_2\{4\} = \sqrt[4]{-c_2\{4\}} \tag{4.20}$$

4.2.3 Two Particle Differential Flow

In the flow methods explained above, all of the particles were used in the calculation; however in the differential flow method, only a certain number of particles is used e.g. particles in a particular p_T interval. For the reference flow, all the particles are labeled as Reference Particles (RFPs) and the calculations are similar to last section. But in the differential flow, each particle we are interested in, is marked as a Particle of Interest (POI). The two-particle azimuthal correlation (or reduced two-particle correlation) for differential elliptic flow is then:

$$\langle 2' \rangle = \langle e^{2i(\psi_1 - \phi_2)} \rangle = \frac{1}{m_p M - m_q} \sum_{i=1}^{m_p} \sum_{j=1}^{M} e^{2i(\psi_i - \phi_j)} \tag{4.21}$$

where m_p is POI number, M is the number of RFPs and $m_q = m_p + M$; ψ_i is the azimuthal angle of i-th POI and ϕ_j is the azimuthal angle of j-th RFPs. p_2 and q_2 are defined as:

$$p_2 \equiv \sum_{i=1}^{m_p} e^{(2i\psi_i)} \tag{4.22}$$

$$q_2 \equiv \sum_{i=1}^{m_q} e^{(2i\psi_i)} \tag{4.23}$$

Now the definition of reduced 2-particle correlation is:

$$\langle 2' \rangle = \frac{p_2 Q^* - m_q}{m_p M - m_q} \tag{4.24}$$

The average of $\langle 2' \rangle$ over N events is:

$$\langle\langle 2'\rangle\rangle = \frac{\sum_{i=1}^{N}(w_{\langle 2'\rangle})_i\langle 2'\rangle_i}{\sum_{i=1}^{N}(w_{\langle 2'\rangle})_i} \tag{4.25}$$

the definition of event weight is:

$$w_{\langle 2'\rangle} \equiv m_p M - m_q \tag{4.26}$$

so the differential second order cumulant is:

$$d_2\{2\} = \langle\langle 2'\rangle\rangle \tag{4.27}$$

Finally the differential elliptic flow for 2-particle cumulant is derived:

$$v_2'\{2\} = \frac{d_2\{2\}}{\sqrt{c_2\{2\}}} \tag{4.28}$$

The Four particle differential flow can be obtained in a similar manner.

4.3 Fluctuation and Non-flow effects

2-particle and 4-particle methods are affected by the flow fluctuation and non-flow effects differently. I will briefly summarize their influences on two methods. The elliptic flow is biased due to flow fluctuation and for $v_2\{2\}$, it can be shown [13]:

$$v_2\{2\} = (\langle v_2\rangle^2 + \sigma_{v_2}^2)^{1/2} \approx \langle v_2\rangle + \frac{1}{2}\frac{\sigma_{v_2}^2}{\langle v_2\rangle} \tag{4.29}$$

where $\langle v_2\rangle$ is the value of interest of the elliptic flow and $\sigma_{v_2}^2$ is the variance of v_2. Similarly, for $v_2\{4\}$ it can be shown [13]:

$$v_2\{4\} = (\langle v_2\rangle^4 - 2\sigma_{v_2}^2\langle v_2\rangle^2 - \sigma_{v_2}^4)^{1/4} \approx \langle v_2\rangle - \frac{1}{2}\frac{\sigma_{v_2}^2}{\langle v_2\rangle} \tag{4.30}$$

Non-flow is characterized by back-to-back particles, for example, originating from a resonant decay. The non-flow can affect $\langle v_2\rangle$, which can increase the value of elliptic flow, but it cannot influence the higher order of cumulants because non-flow is limited with the correlation of small number of particles ($\delta_{v_2\{2\}} \sim \frac{1}{M}$, $\delta_{v_2\{4\}} \sim \frac{1}{M^3}$ and so on). Accounting for the contribution of non-flow effects, $v_2\{2\}$ can be written as [13]:

$$v_2\{2\} = \sqrt{\langle {v_2}^2\rangle} + \delta_{v_2} \tag{4.31}$$

where δ_{v_2} is the statistical error of elliptic flow. Including fluctuations and non-flow, the difference between two methods is:

$$v_2\{2\} - v_2\{4\} \sim \frac{\sigma_{v_2}^2}{\langle v_2\rangle} + \delta_{v_2} \tag{4.32}$$

Chapter 5

5 Results

All the analyses in this thesis have been obtained by a C++ analysis program which utilizes the ROOT framework. The data used for comparison are from Pb-Pb collisions from the ATLAS detector with $\sqrt{s_{NN}} = 2.76$ TeV [7]. The number of events used in this analysis, are 11,154,977.

5.1 Event Plane Method

As mentioned in the previous chapter, it is not possible to measure the reaction plane. To solve this problem, event-by-event reconstruction of the event plane, ψ_2, is done. The next step is the construction of $\phi - \psi_2$. In the appendix A, the two-dimensional histograms of $\phi - \psi_2$ vs p_T are shown. We then divide each centrality class into 0.2 GeV p_T bins and project resulting distribution on $\phi - \psi_2$ axis. These projections for 30-40% centrality events are given in appendix B. For the other different centrality we can use the same method. The azimuthal distribution with some assumption is:

$$\frac{dN}{d\phi} \propto 1 + 2v_2 \cos[2(\phi - \psi_2)] \tag{5.1}$$

From the azimuthal distribution, v_2 can be extracted using a fit. The figure 5.1 shows the elliptic flow of the analysis of ALICE data compared to the ATLAS data for different centralities. As we can see, the elliptic flow has the maximum value at the point around $p_T = 3$ GeV. In peripheral collision, because of the few tracks in TPC, there is a strong autocorrelation, so the flow from event plane method in TPC is higher than the flow measured by ATLAS. This is a limit of the method. In other event plane analysis in ALICE the forward detector V0 has been used to avoid these correlations but then one has to make a large correction for resolution as the V0 detector is poorly segmented. In my analysis the main focus was on the cumulant analysis and so nothing more has been done to improve the event plane analysis in peripheral events.

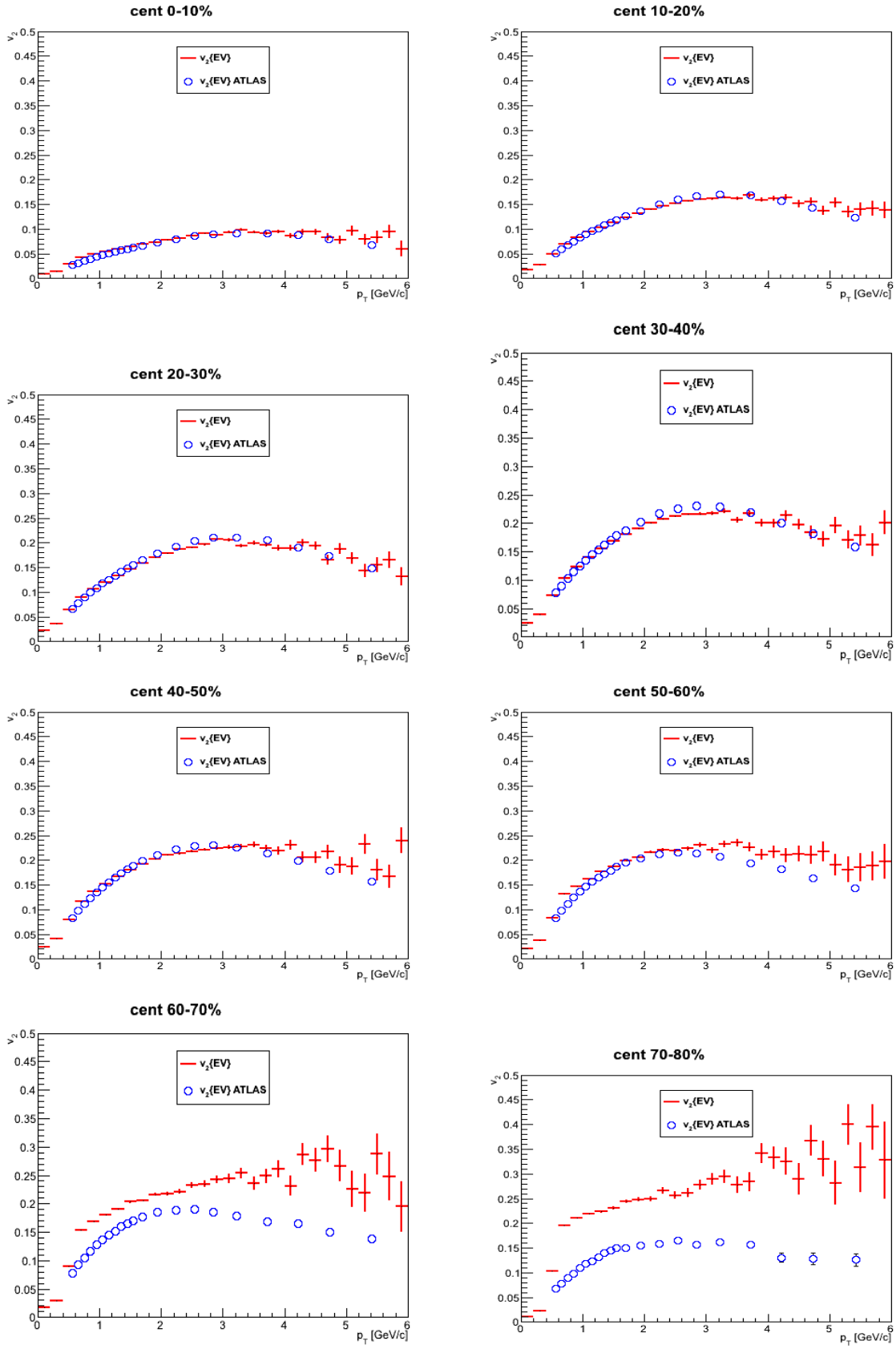

Figure 5.1: The elliptic flow of ALICE data compared to ATLAS results for charged particles in Pb-Pb collision at $\sqrt{s_{NN}} = 2.76$ TeV for eight different centralities between 0% to 80%.

5.2 Cumulant method

The other method which was explained in the previous chapter was two and four particle cumulant to extract the elliptic flow. The figure 5.2 shows the v_2 as a function of centrality.

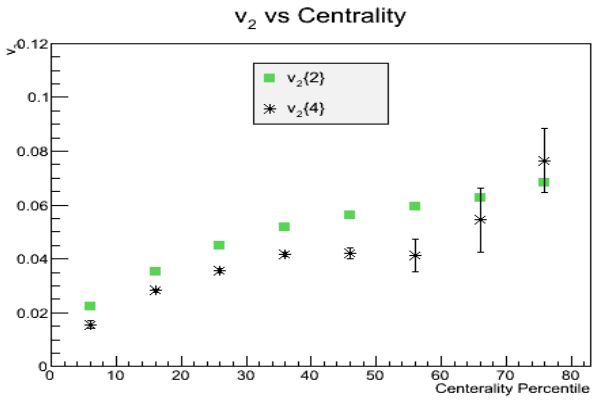

Figure 5.2: Integrated 2 and 4-particle elliptic flow for different centralities.

The figures 5.3 and 5.4 show the $v_2\{2\}$ and $v_2\{4\}$ as a function of p_T. The graphs only show the low transverse momentum range where the method is stable. For 4-particle cumulants the method was sometimes unstable at higher p_T. This was not understood and unfortunately there was no time to investigate this in great detail. One could observe that the cumulants did not converge when more events were used but would sometimes jump significantly after several thousands events. For 2-particle cumulants this problem of convergence was never observed. This high p_T is even more complicated to study as the bulk of the particles are produced at low p_T.

The statistical error bars are small so they are only visible for a few points. It was evaluated from the variation of the cumulants.

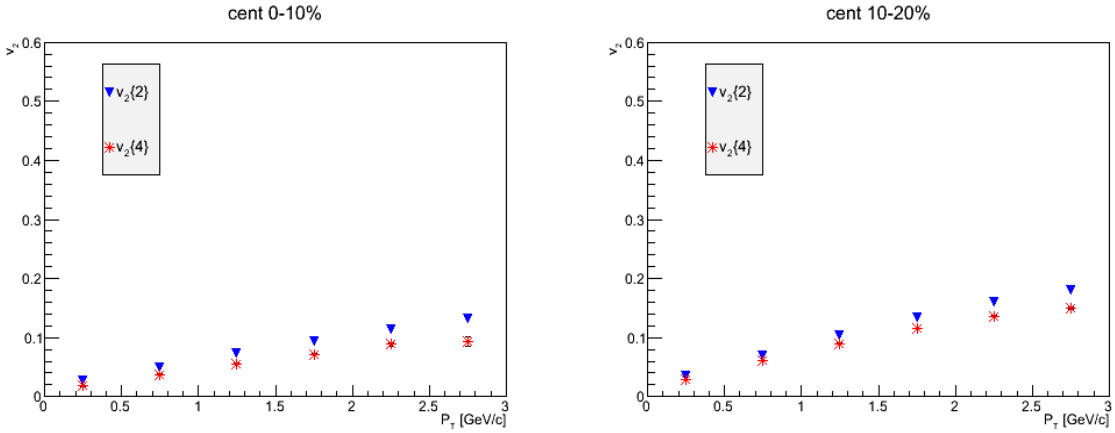

Figure 5.3: The differential elliptic flow as a function of p_T for different cetralities.

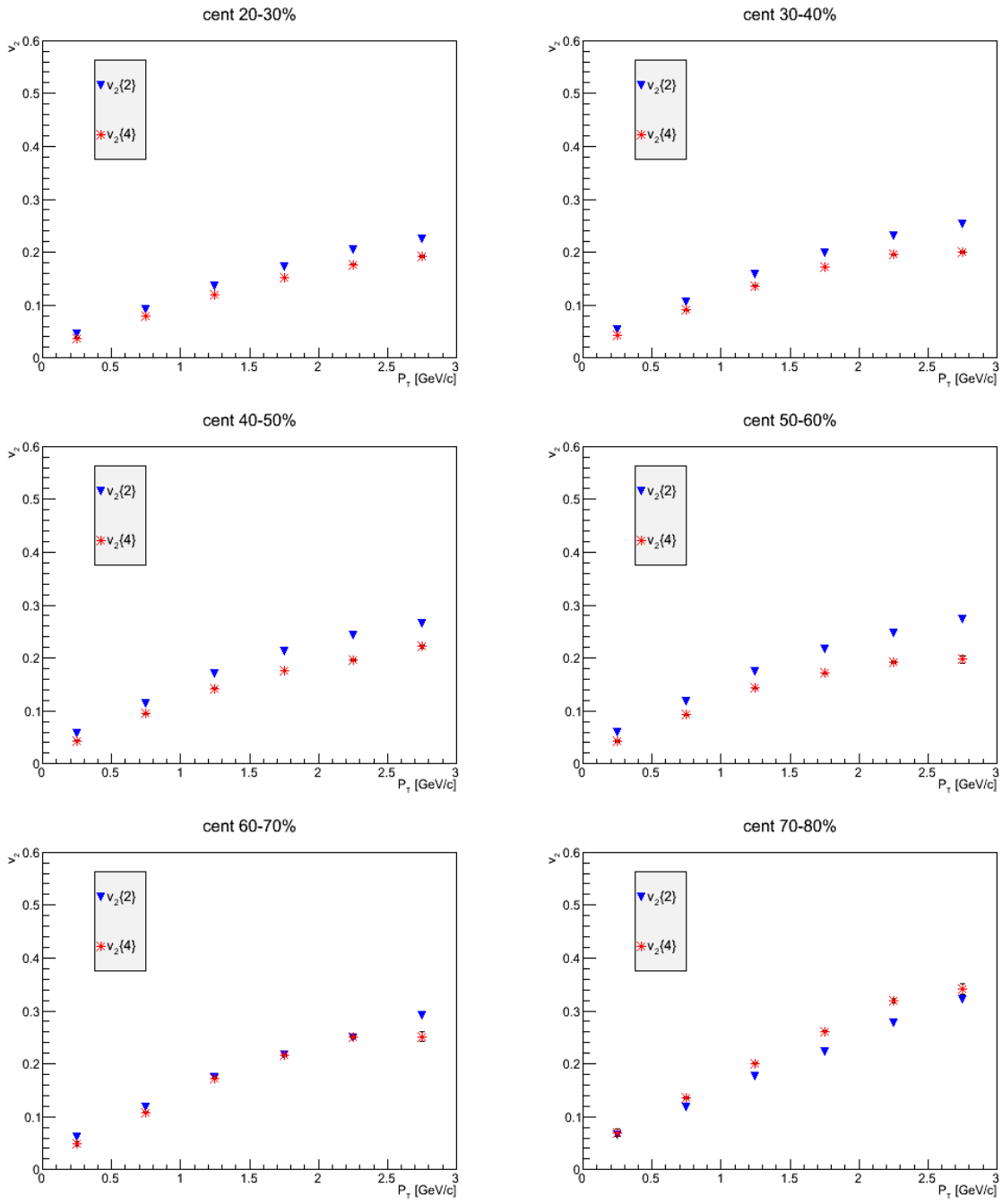

Figure 5.4: The differential elliptic flow as a function of p_T for different cetralities.

From figure 5.5 we see that both 2-particle cumulant and 4-particle cumulant v_2's increase when going to peripheral collision.

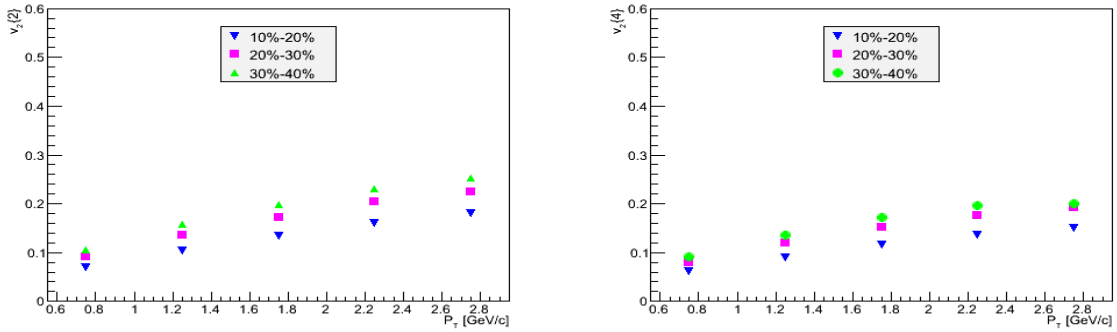

Figure 5.5: The differential elliptic flow as a function of p_T for different cetralities.

Figure 5.6 and 5.7 show the two-particle differential flow compared to elliptic flow of event plane method and 4-particle differential flow for different centralities.

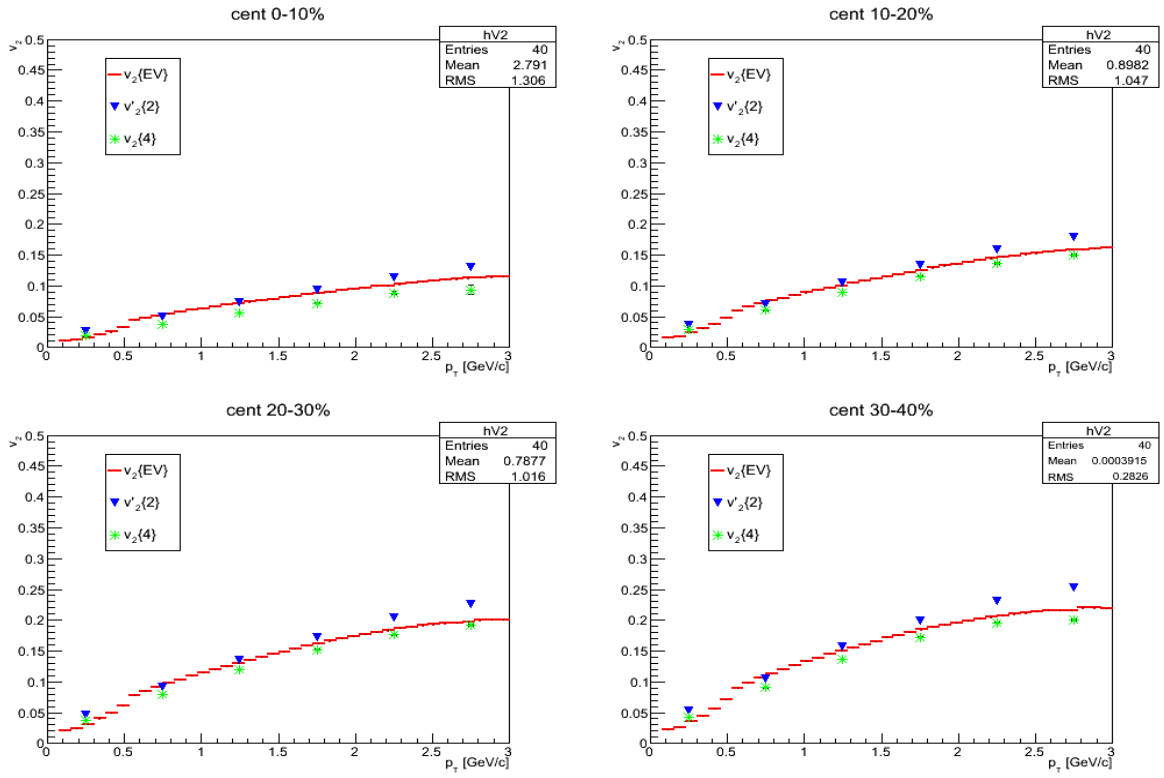

Figure 5.6: The 2-particle differential flow as a function of p_T for different cetrallities between 0% to 60%, compared to v_2 from event plane method and 4-particle differential flow.

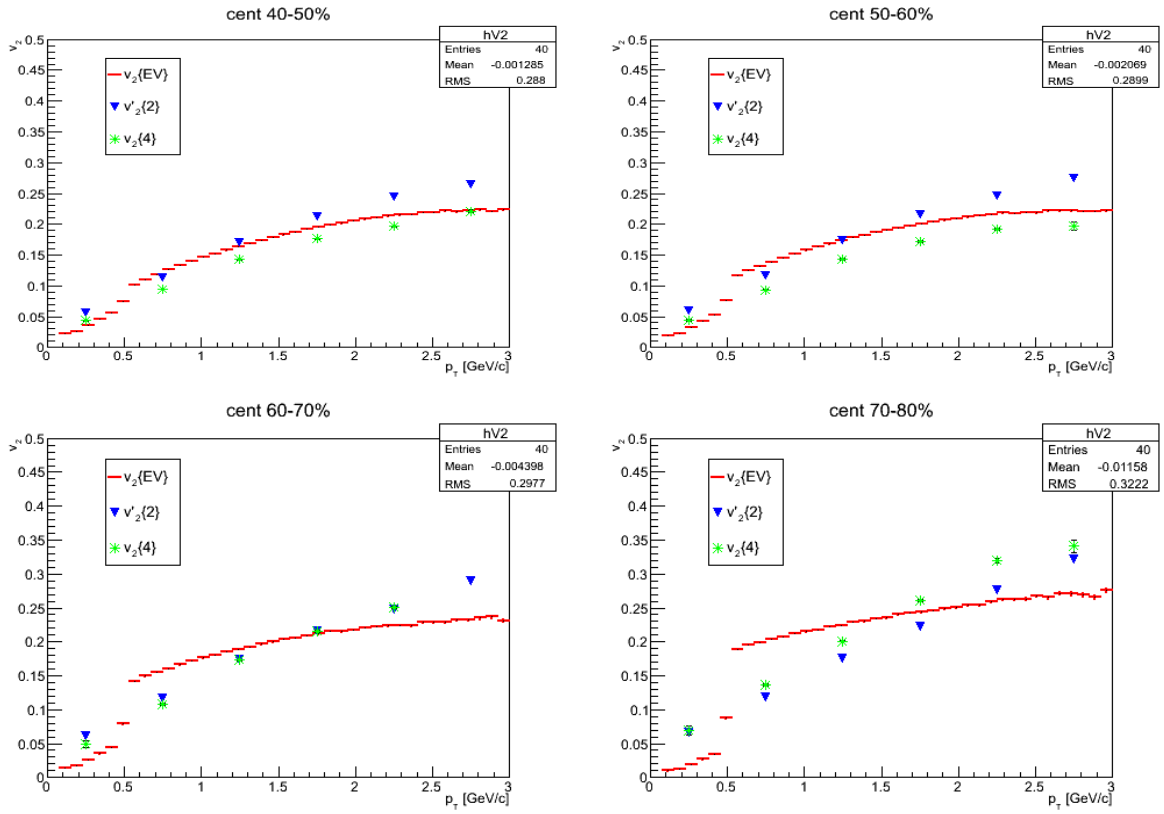

Figure 5.7: The 2-particle differential flow as a function of p_T for different cetrallities between 60% to 80%, compared to v_2 from event plane method and 4-particle differential flow.

5.3 Conclusions

It was shown that the elliptic flow of 2-particle cumulant is higher than the elliptic flow of 4-particle cumulant due to particle fluctuations and non-flow effects, especially in peripheral collisions. As it was mentioned in the previous chapter, 2-particle cumulant has a positive value for particle fluctuation and 4-particle cumulant has a negative value. In other words, they are affected by particle fluctuation in the opposite directions. In addition, the elliptic flow of 2-particle cumulant is also influenced by the non-flow effects due to the low multiplicity. On the other hand, v_2 obtained from 4-particle cumulant is very insensitive to non-flow effects.

The last part of the thesis shows the comparison of elliptic flow from three different methods, namely the event plane, 2-particle cumulant and 4-particle cumulant. As we have seen, the elliptic flow of event plane is in between the elliptic flow of 2-particle cumulant and 4-particle cumulant, because the event plane is not affected by the particle fluctuations. Elliptic flow of event plane is, however, enhanced by the autocorrelation of particles.

5.4 Outlook

I have done elliptic flow in low transverse momentum and got good results. I tried to measure elliptic flow of cumulat method after transverse momentum at 3 GeV but it had problem that elliptic flow of 4-particle cumulant was larger than elliptic flow of 2 particle cumulant. The elliptic flow of event plane method gives us good results up to $p_t = 6$ GeV but the next step for this thesis can be measuring elliptic flow of cumulant method for higher transverse momentum from TPC data.

6 Appendices

6.1 A

The reconstruction of $\phi - \psi_2$ for transverse momentum between 0 to 6 GeV for different centrality is shown below:

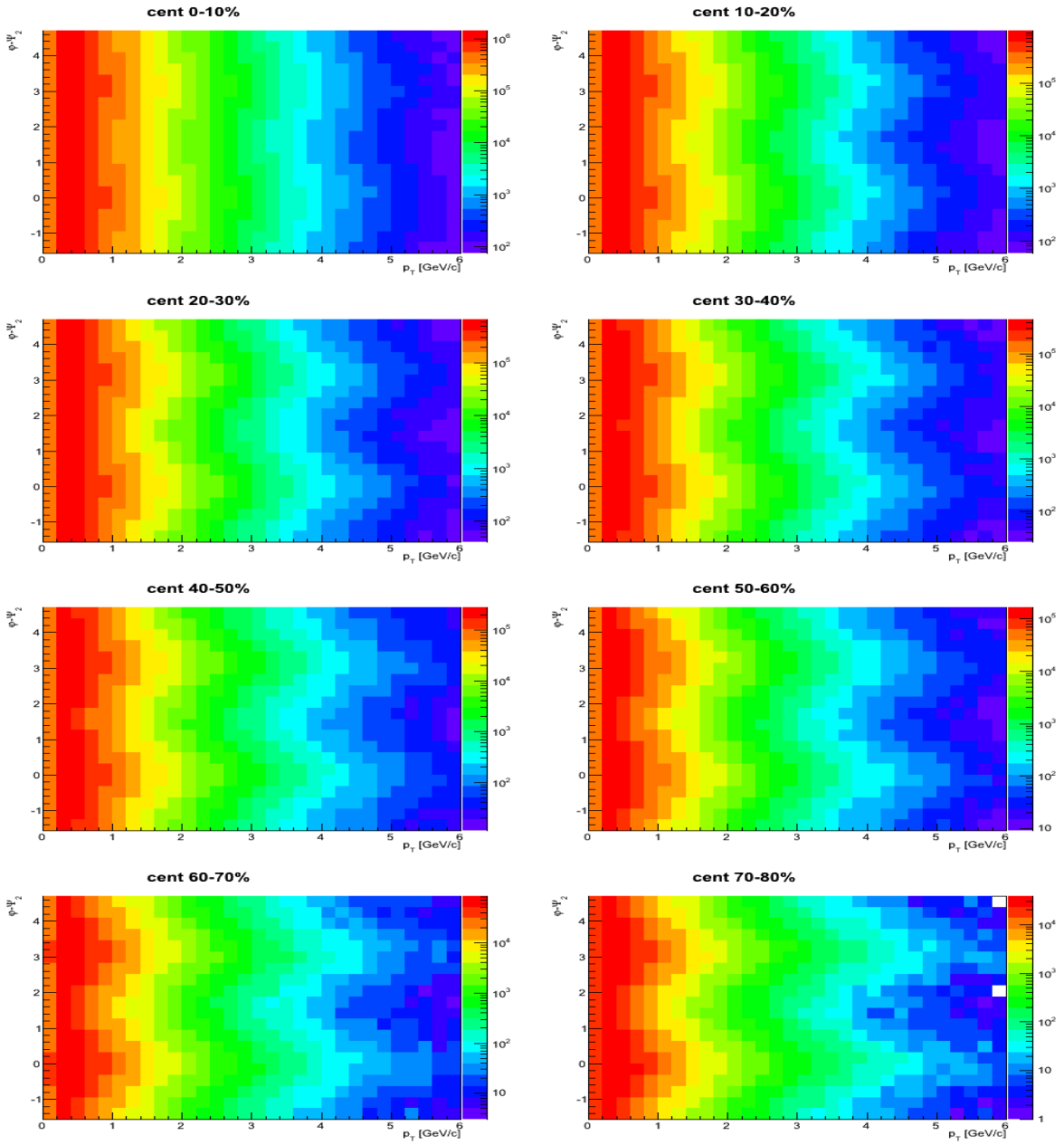

Figure A

6.2 B

The azimuthal distribution relative to $\phi - \psi_2$ for different centrality 30%-40% between $0 \leq p_t \leq 6$ GeV with every 0.2 GeV differences.

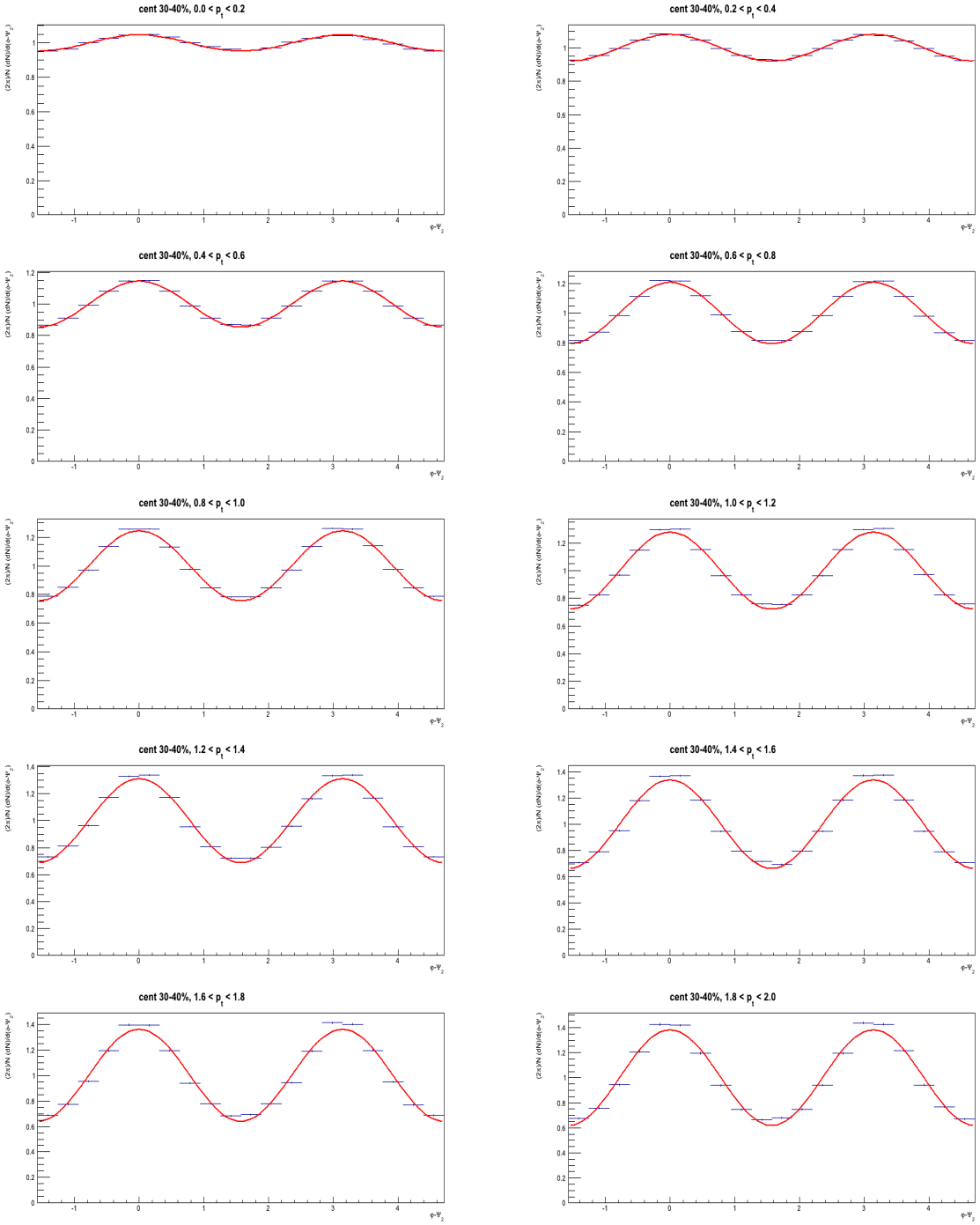

Figure B

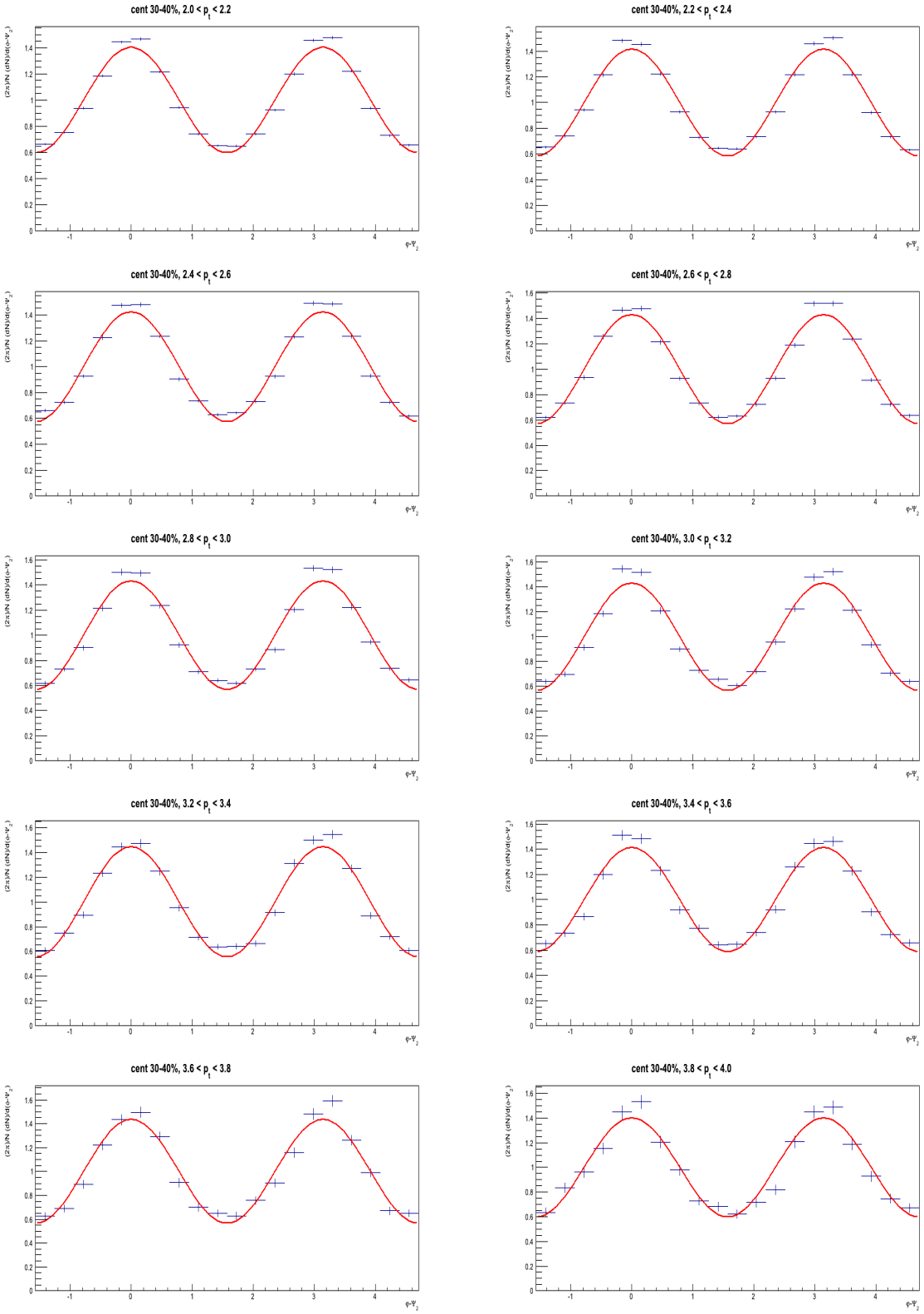
cent 30-40%, 2.0 < p_t < 2.2
cent 30-40%, 2.2 < p_t < 2.4
cent 30-40%, 2.4 < p_t < 2.6
cent 30-40%, 2.6 < p_t < 2.8
cent 30-40%, 2.8 < p_t < 3.0
cent 30-40%, 3.0 < p_t < 3.2
cent 30-40%, 3.2 < p_t < 3.4
cent 30-40%, 3.4 < p_t < 3.6
cent 30-40%, 3.6 < p_t < 3.8
cent 30-40%, 3.8 < p_t < 4.0

Figure B

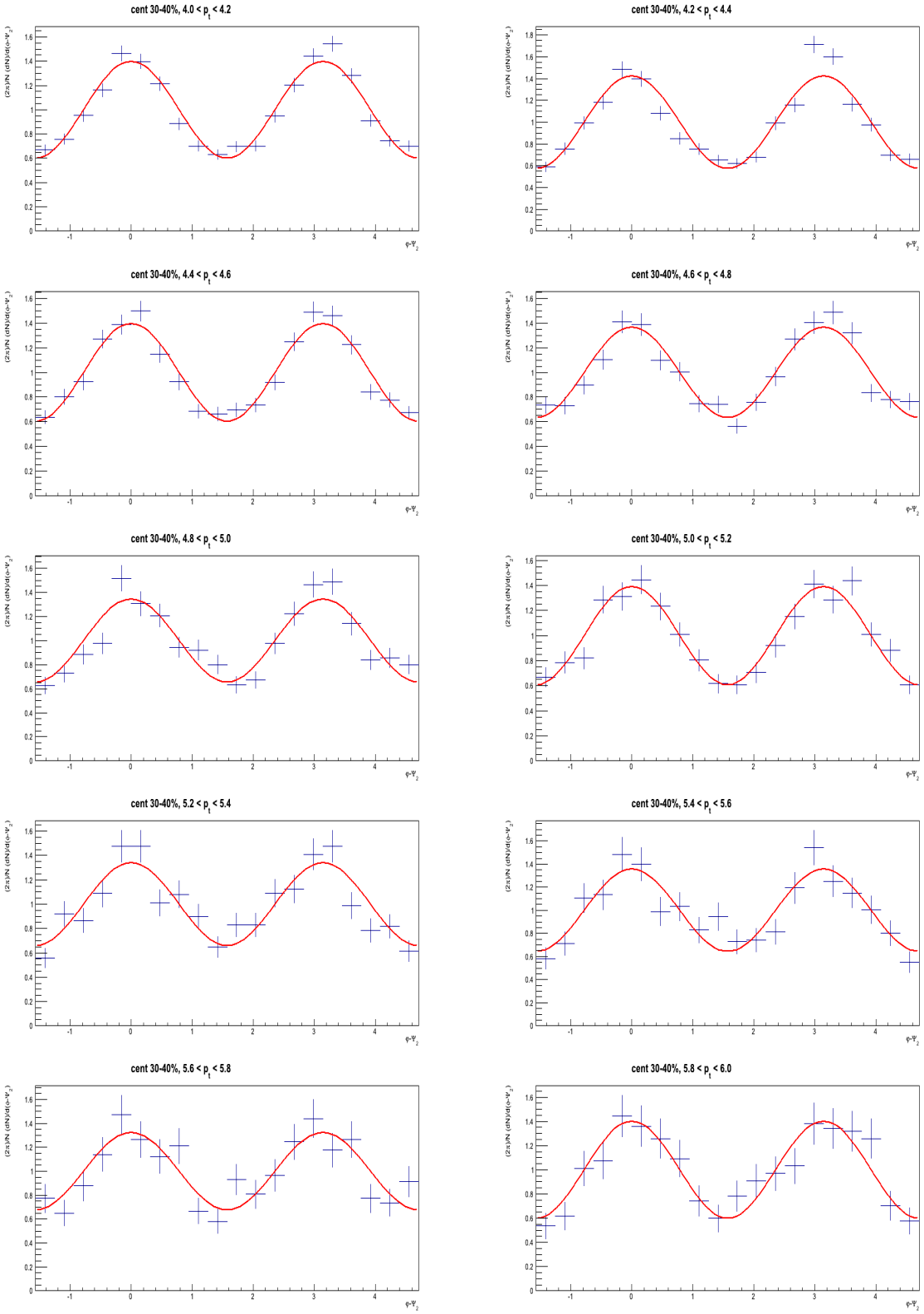
cent 30-40%, 4.0 < p_t < 4.2
cent 30-40%, 4.2 < p_t < 4.4
cent 30-40%, 4.4 < p_t < 4.6
cent 30-40%, 4.6 < p_t < 4.8
cent 30-40%, 4.8 < p_t < 5.0
cent 30-40%, 5.0 < p_t < 5.2
cent 30-40%, 5.2 < p_t < 5.4
cent 30-40%, 5.4 < p_t < 5.6
cent 30-40%, 5.6 < p_t < 5.8
cent 30-40%, 5.8 < p_t < 6.0

Figure B

References

[1] S.Voloshin and Y.Zhang, *Flow Study in Relativistic Nuclear Collision by Fourier Expansion of Azimuthal Particle Distribution*, arXiv:hep-ph/940728v1,1994.

[2] K Admodt et al., *Elliptic flow of charged particles in Pb-Pb collisions* $\sqrt{s_{NN}} = 2.76$ TeV, Phys.Rev.Lett., vol. 105,pp. 252302, 2010.

[3] A.Bilandzic., *Anisotropic flow of charged particles at* $\sqrt{s_{NN}} = 2.76$ TeV *measured with the ALICE detector*, J.Phys.G:Nucl.Part.38 (2011)124052.

[4] A.Bilandzic, R.Snelling, S.Voloshin, *Flow analysis with cumulants: direct calculations*, arXiv:1010.0233v2[nucl-ex] 17Oct2011.

[5] N.Borghini , P.M.Dinh , J.Ollitrault , *Flow analysis from multiple azimuthal correlation* , Phys.Rev.vol64, 2001.

[6] E.Simili, *Elliptic Flow Measurement at ALICE*, ISBN:978-90-393-4839-0, 2008.

[7] The ATLAS Collaboration, *Measurement of the psudorapidity and transverse momentum dependence of the elliptic flow of charged particles in lead-lead collision at* $\sqrt{s_{NN}} = 2.76$ TeV *with the ATLAS detector*, arXiv:1108.6018v2[hep-ex], 2011.

[8] E.Simili, *Elliptic Flow Measurement at ALICE*, ISBN:978-90-393-4839-0, 2008.

[9] N.Borghini, P.M.Dinh, J.Ollitrault, Phys.Rev.C 62, 034902 (2000)

[10] N.Borghini, P.M.Dinh, J.Ollitrault, Phys.Rev.C 63, 054906 (2001)

[11] N.Borghini, P.M.Dinh, J.Ollitrault, Phys.Rev.C 64, 034904 (2002)

[12] B.Alver, G.Roland, *Collision geometry fluctuations and triangular flow in heavy-ion collisions*, Phys.Rev.C81:054905,2010.

[13] S.Voloshin, A.M.Poskanzer, R.Snellings, *Collective phenomena in non-central nuclear collisions*, arXiv:0809.2949v2[nuc1-ex], 30 Oct 2008.

[14] K.Admodt et al., *Charged-particle multiplicity density at mid-rapidity in central Pb-Pb collisions at* $\sqrt{s_{NN}} = 2.76$ TeV, Phys.Rev.Lett.,vol.105,pp. 252301, 2010.

[15] http://www.lctpc.org/e8/e57671/, *Lctpc, a time projection chamber for the future linear collider.*

[16] B.Alver, M.Baker, C.Loizides, and P.Steinberg, *The PHOBOS Glauber Monte Carlo*, arXiv:0805.4411[nuc1-ex], 2008.

[17] http://en.wikipedia.org/wiki/File:Standard_Model_of_Elementary_Particles.svg

[18] Gunnar S Bali, *QCD forces and heavy quark bound states*, Phs. Rept., vol.343,pp.1-136, 2001.

[19] https://www.phy.duke.edu/research/NPTheory/QGP/index.php

[20] http://i63.photobucket.com/albums/h136/blueice760/QCDPhasendiagram1.jpg

[21] http://www.quantumdiaries.org/wp-content/uploads/2011/02/FlowPr.jpg

[22] http://en.wikipedia.org/wiki/File:LHC.svg

[23] http://www.isgtw.org/images/2008/ALICE_diagram.jpg

[24] http://media.monstersandcritics.com/galleries/2619124_29974/0243833355085.jpg

[25] http://inspirehep.net/record/871528/files/plots_geometry.png

[26] http://ars.els-cdn.com/content/image/1-s2.0-S0146641008001336-gr1.jpg